Clays and Clay Minerals, Vol. 61, No. 1, 57–74, 2013.

SPECTRAL AND HYDRATION PROPERTIES OF ALLOPHANE AND IMOGOLITE

Janice L. Bishop[1,*], Elizabeth B. Rampe[2], David L. Bish[3], Zaenal Abidin[4,5], Leslie L. Baker[6], Naoto Matsue[4], and Teruo Henmi[4]

[1] Carl Sagan Center, SETI Institute and NASA-ARC, 189 Bernardo Avenue, Mountain View, CA 94043, USA
[2] NASA-JSC, Mail Code KA, Houston, TX 77058, USA
[3] Department of Geological Sciences, Indiana University, 1001 E. 10th St., Bloomington, IN 47405, USA
[4] Faculty of Agriculture, Ehime University, Tarumi 3-5-7, Matsuyama 790-8566, Japan
[5] Inorganic Chemistry Laboratory, Department of Chemistry, Faculty of Mathematics and Natural Science, Bogor Agricultural University, Jl. Agatis Kampus IPB Darmaga, Bogor, West of Java, 16680, Indonesia
[6] Department of Plant, Soil and Entomological Sciences, University of Idaho, 875 Perimeter Drive MS 2339, Moscow, ID 83844, USA

Abstract—Allophane and imogolite are common alteration products of volcanic materials. Natural and synthetic allophanes and imogolites were characterized in the present study in order to clarify the short-range order of these materials and to gain an understanding of their spectral properties. Spectral analyses included visible/near-infrared (VNIR), and infrared (IR) reflectance of particulate samples and thermal-infrared (TIR) emissivity spectra of particulate and pressed pellets. Spectral features were similar but not identical for allophane and imogolite. In the near-infrared (NIR) region, allophane spectra exhibited a doublet near 7265 and 7120 cm^{-1} (1.38 and 1.40 μm) due to $OH_{2\nu}$, a broad band near 5220 cm^{-1} (1.92 μm) due to $H_2O_{\nu+\delta}$, and a band near 4560 cm^{-1} (2.19 μm) due to $OH_{\nu+\delta}$. Reflectance spectra of imogolite in this region included a doublet near 7295 and 7190 cm^{-1} (1.37 and 1.39 μm) due to $OH_{2\nu}$, a broad band near 5200 cm^{-1} (1.92 μm) due to $H_2O_{\nu+\delta}$, and a band near 4565 cm^{-1} (2.19 μm) due to $OH_{\nu+\delta}$. A strong broad band was also observed near 3200−3700 cm^{-1} (~2.8−3.1 μm) which is a composite of OH_ν, H_2O_ν, and $H_2O_{2\delta}$ vibrations. Visible/near-infrared spectra were also collected under two relative humidity (RH) conditions. High-RH conditions resulted in increasing band strength for the H_2O combination modes near 6900−6930 cm^{-1} (1.45 μm) and 5170−5180 cm^{-1} (1.93 μm) in the allophane and imogolite spectra due to increased abundances of adsorbed H_2O molecules. Variation in adsorbed H_2O content caused an apparent shift in the bands near 1.4 and 1.9 μm. A doublet H_2O_δ vibration was observed at 1600−1670 cm^{-1} (~6.0−6.2 μm) and a band due to OH bending for O_3SiOH was observed at ~1350−1485 cm^{-1} (~6.7−7.4 μm). The Si−O−Al stretching vibrations occurred near 1030 and 940 cm^{-1} (~9.7 and 10.6 μm) for allophane and near 1010 and 930 cm^{-1} (~9.9 and 10.7 μm) for imogolite. OH out-of-plane bending modes occurred near 610 cm^{-1} (16.4 μm) for allophane and at 595 cm^{-1} (16.8 μm) for imogolite. Features due to Si−O−Al bending vibrations were observed at 545, 420, and 335 cm^{-1} (~18, 24, and 30 μm) for allophane and at 495, 415, and 335 cm^{-1} (~20, 24, and 30 μm) for imogolite. The emissivity spectra were obtained from pressed pellets of the samples, which greatly enhanced the spectral contrast of the TIR absorptions. Predicted NIR bands were calculated from the mid-IR fundamental stretching and bending vibrations and compared with the measured NIR values. Controlled-RH X-ray diffraction (XRD) experiments were also performed in order to investigate changes in the mineral structure with changing RH conditions. Both allophane and imogolite exhibited decreasing low-angle XRD intensity with increasing RH, which was probably a result of interactions between H_2O molecules and the curved allophane and imogolite structures.

Key Words—Allophane, Emission Spectroscopy, Imogolite, Reflectance Spectroscopy, XRD.

INTRODUCTION

Allophane and imogolite frequently occur together as clay-sized soil components derived from volcanic ash and pumice or as alteration products of basaltic saprolite (*e.g.* Henmi and Wada, 1976; Wada, 1987; Parfitt, 2009). These two aluminosilicates form under related geochemical conditions, but they have different structures. They are listed as minerals by the International Mineralogical Association (http://www.ima-mineralogy.org/), but are considered non-mineral phases by The Clay Minerals Society (http://www.clays.org/GLOSSARY/GlossIntro.html) due to their lack of sufficiently well defined structures. The ideal chemical formula for imogolite is $(OH)_3{\cdot}Al_2O_3{\cdot}SiOH$ (Parfitt, 2009). The chemical formula of allophane is variable and has been given as $1.0–2.0SiO_2{\cdot}Al_2O_3{\cdot}2.5–3.0H_2O$ (Wada, 1987). Both minerals readily adsorb H_2O and hold significantly more H_2O per formula unit under moist conditions than under dry conditions. Previous studies have examined in detail the mineral structure, chemistry, and infrared transmission spectra (*e.g.* Henmi and Wada, 1976; Farmer *et al.*, 1977; Parfitt *et al.*, 1980).

* E-mail address of corresponding author:
jbishop@seti.org
DOI: 10.1346/CCMN.2013.0610105

The present study builds on this previous work to measure and analyze the spectral properties of allophane and imogolite by using reflectance spectra in the VNIR and mid-IR regions and emissivity spectra in the TIR region. These reflectance and emissivity spectra are necessary for remote mineral identification, and this study will enable inclusion of allophane and imogolite in spectral libraries. This will further allow for their consideration in remote sensing investigations on Earth and other planets. Both natural samples from Japan (Figure 1) and synthetic samples are characterized in the present study. In order to examine the effects of humidity and changing hydration state of the samples on the spectral features, XRD data have been acquired over a range of relative humidity (RH) conditions and VNIR reflectance spectra were obtained under two RH conditions. The influence of hydration level on the IR and XRD signatures are especially important for remote sensing studies of allophane and imogolite on Earth and the identification of these components on Mars and other planetary bodies that have a much drier environment.

BACKGROUND

Allophane and imogolite form primarily through alteration of volcanic ash and most commonly occur where ash is an important soil component (*e.g.* Fieldes, 1955; Yoshinaga and Aomine, 1962; Wada, 1967; Wada *et al.*, 1972; Henmi and Wada, 1976; Nagasawa, 1978; Theng *et al.*, 1982; Parfitt, 2009). X-ray diffraction (*e.g.* van der Gaast *et al.*, 1985; Parfitt, 1990), IR spectroscopy (Russell *et al.*, 1969; Cradwick *et al.*, 1972; Henmi and Wada, 1976; Farmer *et al.*, 1979; Parfitt *et al.*, 1980), electron microscopy (Henmi and Wada, 1976), NMR (Shimizu *et al.*, 1988), and chemical (Henmi and Wada, 1976) and thermal (Henmi, 1980;

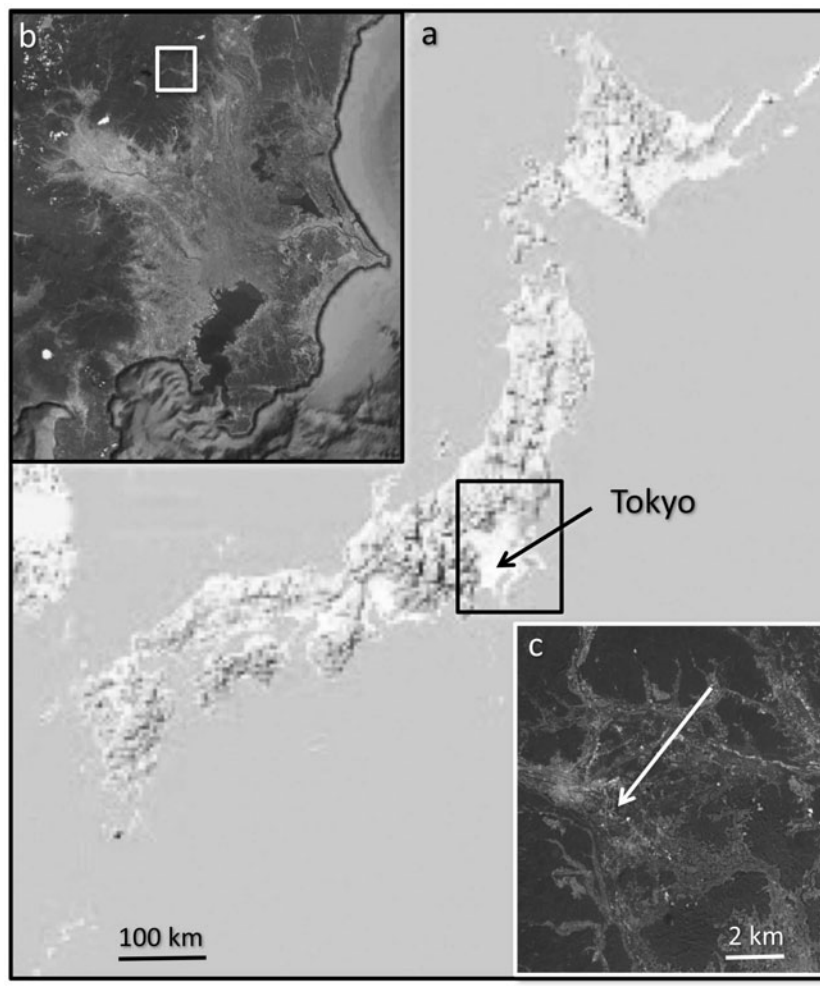

Figure 1. Map of sample location at Imaichi, Nikko, near Tokyo (36º43′16.276″N, 139º42′14.688″E), where natural samples were collected: (a) map of Japan; (b) region NW of Tokyo; and (c) sample location. Image credit: 2012 CNES/SPOT, Google Earth, Feb. 10, 2012.

https://doi.org/10.1346/CCMN.2013.0610105 Published online by Cambridge University Press

MacKenzie *et al.*, 1989) studies of these minerals have led to a general understanding of their character. These studies have shown that allophane is nearly X-ray amorphous and has a hollow-sphere structure with a diameter of 3.5−5 nm, whereas imogolite has a discrete XRD pattern and a tubular structure. Thus, allophane has only short-range ordering, but imogolite has long-range ordering in one dimension. Although these materials are poorly and para-crystalline, they have distinct and recognizable XRD patterns (*e.g.* van der Gaast *et al.*, 1985). Allophane has a molar Si/Al ratio between 0.5 and 1; imogolite, near 0.5. Henmi and Wada (1976) found a change in the Al configuration as volcanic glass altered: Al is largely 4-coordinated in volcanic glass, 4- and/or 6-coordinated in allophane, and mostly 6-coordinated in imogolite. Allophane and imogolite can be identified in soils by their dissolution in 0.2 M oxalate-oxalic acid at pH 3 (Wada, 1987).

Synthesis of allophane and imogolite can be achieved by heating solutions of orthosilicic acid and hydroxy-Al cations at 95−100ºC (Farmer *et al.*, 1977; Wada *et al.*, 1979; Farmer *et al.*, 1983). Both mineraloids form together in about 1 week, although imogolite is favored at lower Si/Al ratios and a pH near 5, whereas allophane is favored at pH values of 6−8. However, imogolite-like products were also found up to pH 8 for Si/Al ratios $\leqslant 0.25$ (Farmer *et al.*, 1979). Combined synthesis experiments and molecular orbital calculations showed that Ca and Na cations in solution greatly facilitate the formation of allophane and suppress the formation of imogolite (Abidin *et al.*, 2007a). The alkali metal cations in solution inhibit imogolite formation for Ca/Al >10 and Na/Al > 50 as shown by IR and XRD analyses.

Transmittance spectra indicate a shift in the Si−O stretching vibration from ~1000 cm^{-1} for silica gel to near 940 cm^{-1} for allophane and imogolite (Farmer *et al.*, 1979). These spectra exhibit a shoulder near 1000 cm^{-1} for imogolite that is close to the band for most forms of opal and silica gel. Farmer *et al.* (1979) further observed that the Si−O stretching vibration is generally narrower in natural samples and broader in spectra of synthetic ones. Those authors suggested that this is due to a limited range of Si−O bond environments in natural samples. Cradwick *et al.* (1972) interpreted the IR spectra to indicate a structure composed of isolated orthosilicate groups with their Si to apical O bonds perpendicular to the axis of the fiber.

The structure of imogolite is based on a gibbsite-like sheet made up of Si−O−Al and Al−O−Al bonds that is curled in one direction (Figures 2a, 3a,c); Si−O−Si bonds normally are not observed (Wada, 1987). Imogolite forms elongated fibers up to 1 μm long with diameters of <2 nm (Wada, 1989). In contrast, allophane is composed of similar sheets that curl on three edges (Figures 2b, 3b,d), have diameters of ~3.5−5 nm, and tend to form globular aggregates (Wada and Wada, 1977). The structures of imogolite and allophane were examined in more detail recently using molecular orbital calculations (Abidin *et al.*, 2007a; Creton *et al.*, 2008a, 2008b; Konduri *et al.*, 2006; Tamura and Kawamura, 2002) and density functional theory modeling (Alvarez-Ramirez, 2007; Demichelis *et al.*, 2010; Guimarães *et al.*, 2007). Al−O and Si−O bond distances, Al...Al and Si...Si distances, several bond angles, and calculated XRD and IR parameters for model structures were determined for these structures and compared with experimental values for gibbsite (Saalfeld and Wedde, 1974) and imogolite (Cradwick *et al.*, 1972). This work confirmed that imogolite and protoimogolite allophane consist of an interior layer of tetrahedral Si bonded to an outer layer of octahedral Al with OH groups pointing outside and inside the tube (Figure 2a,b). The allophane structure is more complex with clusters of tetrahedral Si and octahedral Al, as well as OH groups pointing outside and inside the sphere (Figure 2b). Imogolite and allophane were found to have similar ideal structures on a unit-cell level based on a gibbsite sheet with orthosilicate clusters (SiO_4) inserted at the vacant octahedral sites such that the O...O distance is shortened in one gibbsite layer and lengthened in the neighboring layer. This causes curling of the structure to produce a tubular structure for imogolite and a nanoball structure for allophane (Abidin *et al.*, 2007a). Reactions performed on allophane surfaces suggest that variations in the Si/Al ratio affect the surface chemistry of the hollow spheres, the development of silanol groups, and the degree of enlargement of pores in the sphere walls (Abidin *et al.*, 2007b).

Relative humidity-controlled XRD studies have been applied to a variety of mineral systems to understand the nature of the interaction of mineral/solid surfaces with H_2O molecules (*e.g.* Bish *et al.*, 1999; Chipera *et al.*, 1997). These measurements, generally performed from 0 to ~95% RH, are particularly sensitive to small changes in surface properties, as exemplified in comparisons of untreated and steam-treated smectites (Bish *et al.*, 1999).

Imogolite and allophane are important soil constituents. They control the physical and chemical character of soils due to their large surface area, unique structures, and high reactivity which enable adsorption of organic molecules and anions such as sulfate and phosphate (*e.g.* Abidin *et al*., 2007a; Parfitt, 2009). Imogolite and allophane frequently occur together as clay components of soils derived from volcanic ash and pumice, largely by alteration of volcanic glass. Favorable environments for the formation of these minerals generally include a moderate water/rock ratio, mildly acidic conditions, and good drainage, where Si and bases are leached from parent material. Imogolite and allophane often form in the subsurface, whereas opaline silica forms at the surface (*e.g.* Wada, 1987). Imogolite was found in the youngest soils, allophane in intermediate soils, and halloysite in the oldest soils in several alteration studies of volcanic tephra (*e.g.* Wada, 1987). Allophane and

https://doi.org/10.1346/CCMN.2013.0610105 Published online by Cambridge University Press

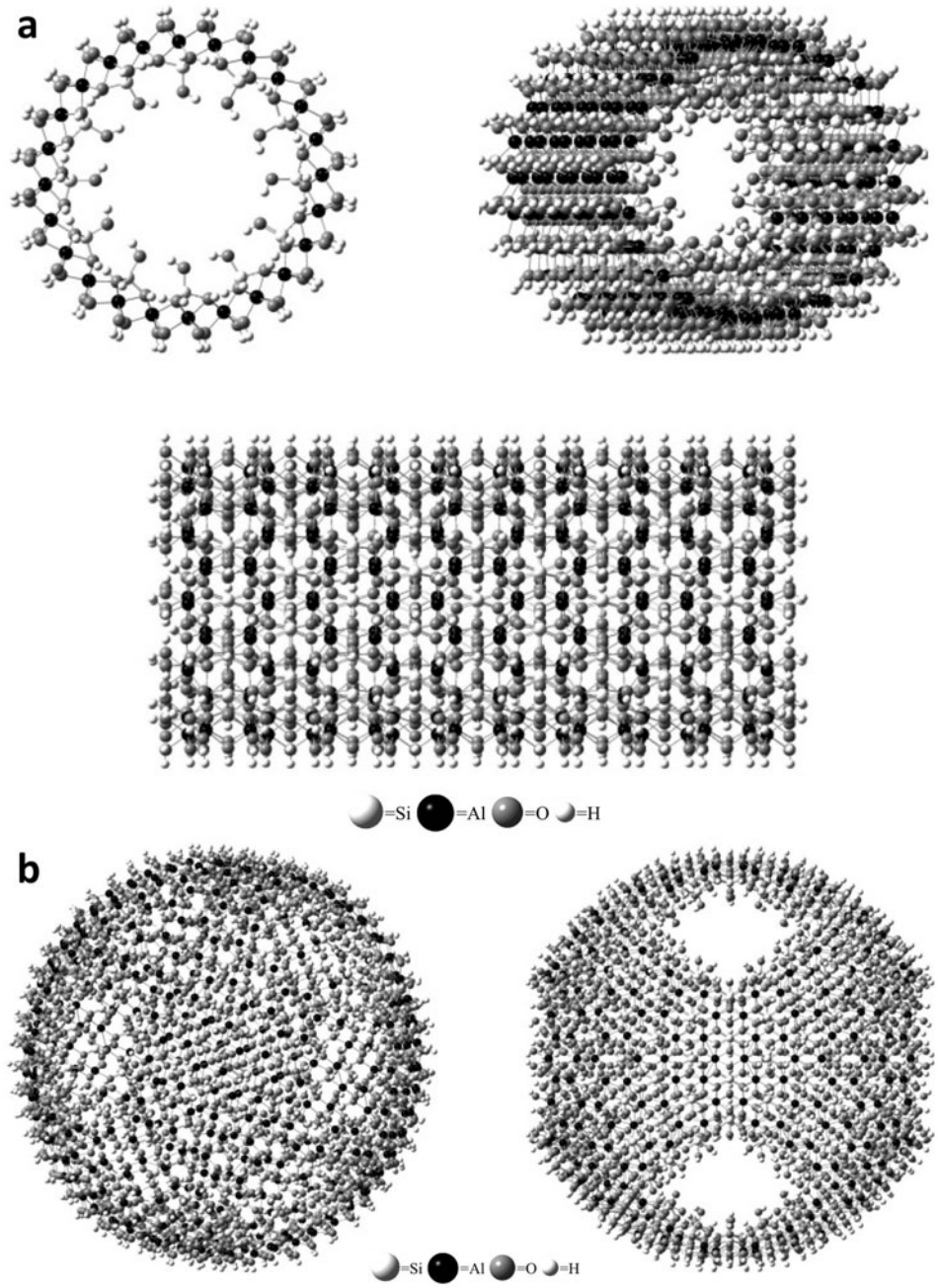

Figure 2. Mineral structures (after Abidin *et al*., 2007a): (a) nano-tube structure of imogolite; (b) nano-ball structure of allophane.

halloysite were found to be more abundant in Hawaiian soils formed from volcanic tephra under less humid conditions, while ferrihydrite and gibbsite were more prevalent in soils formed under tropical conditions (Parfitt *et al.*, 1988). A study of Ecuadorian Andosols found allophane-rich facies in the upper few meters, halloysite-rich facies at 11−15 m depth, and gibbsite at the transition zone (Kaufhold *et al*., 2009, 2010). A study of Andosols from Guadeloupe found that gibbsite and kaolinite were present with allophane in areas that experienced intense leaching of silica (Ndayiragije and Delvaux, 2003). Poorly crystalline minerals such as allophane and imogolite were observed as the favored alteration products in young soils derived from a variety of volcanic ash deposits (Shoji *et al.*, 1993). Therefore, allophane and/or imogolite are indicators of immature soils formed *via* alteration of volcanic material.

Allophane and imogolite also form in the B horizon of Spodosol-like soils derived from Si-rich parent rocks following leaching of the upper E soil horizon and

https://doi.org/10.1346/CCMN.2013.0610105 Published online by Cambridge University Press

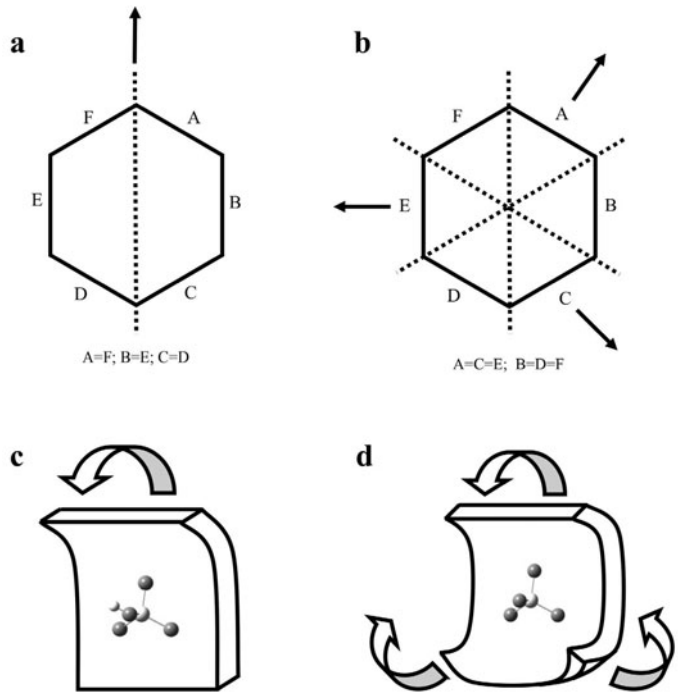

Figure 3. Models of imogolite and allophane symmetry and particle growth patterns: (a) symmetry of imogolite; (b) symmetry of allophane; (c) formation pattern of imogolite; and (d) formation pattern of allophane.

degradation of organometallic complexes in the soil (Buurman and Van Reeuwijk, 1984). Acidic conditions in Sweden were found to favor complexation of Al by organic matter, which inhibits formation of allophane and imogolite (Gustafsson *et al.*, 1998). Al and Fe leached out of the E horizon are bound by organic acids and transferred to the lower B horizon (Lundström *et al.*, 2000). Once microbial activity sufficiently degrades the organometallic complexes, Al becomes free to form gibbsite, imogolite, and allophane (Buurman and Van Reeuwijk, 1984; Gustafsson *et al.*, 1998). Another study of Canadian soils found greater abundances of opaline silica in the surface A horizon and elevated allophane and ferrihydrite in the subsurface B horizon (Kodama and Wang, 1989), similar to studies of volcanic soils. Thus, allophane and imogolite are not entirely unique to volcanic settings because, although uncommon, they can form in soils derived from other parent materials.

METHODS

Samples

The natural imogolite and allophane samples were prepared from pumice that was collected ~30 y ago at Imaichi, Nikko, near Tokyo (Figure 1). This site is located at 36º43′16.276″N, 139º42′14.688″E and the materials here formed by alteration of volcanic material. The imogolite sample was scraped off the outer portion of the pumice. The allophane sample was taken from the remaining inner part of the pumice and had a molar Si/Al ratio of 0.82. Post-collection modification of the samples during storage in the laboratory was assumed to have been minor, no evidence of formation of phyllosilicates was seen in the XRD or IR data. Iron (oxyhydr)oxide phases were removed from the samples using the standard dithionite-citrate-bicarbonate (DCB) treatment described by Mehra and Jackson (1960).

The synthetic imogolite sample was prepared by mixing orthosilicic acid, H_4SiO_4, with aluminum nitrate hexahydrate, $Al(NO_3)_3{\cdot}6H_2O$, to yield an Si/Al ratio of 0.5 for a previous study (Henmi and Huang, 1987). The solution mixtures were titrated with NaOH until an OH/Al molar ratio of 2 was achieved. The Si concentration of the resulting solution was 1.6 mM and the pH was 4.1. The mixture solution was heated at 100ºC for 48 h in an autoclave, then allowed to cool, at which point the pH was 3.0. The product was flocculated by adding saturated sodium chloride solution to the cooled mixture solution. The gelatinous product was centrifuged, dialyzed to remove excess sodium chloride, and freeze-dried to create a powder. Analysis using XRD, scanning electron microscopy (SEM), and differential thermal analysis (DTA) showed the product to be imogolite (Abidin *et al.*, 2008, 2009).

The synthetic allophane sample was prepared using the method described by Montarges-Pelletier *et al.* (2005), with 0.1 M $AlCl_3$ and tetraethyl orthosilicate (TEOS) (5 mL TEOS to 225 mL 0.1 M $AlCl_3$) to produce an Al:Si ratio of 1:1 (Baker and Strawn, 2012). The method was modified to produce an Fe-substituted

https://doi.org/10.1346/CCMN.2013.0610105 Published online by Cambridge University Press

allophane by adding 11.25 mL of 0.1 M $FeCl_3$ to the starting materials to produce a final Fe:Al ratio of 1:20. The gel produced by this synthesis was dialyzed against flowing deionized water and then freeze-dried for analysis.

Reflectance measurements

Reflectance spectra were measured for particulate samples in a horizontal sample dish using a bi-directional VNIR spectrometer and a Nicolet FTIR spectrometer at Brown University's RELAB as in previous studies (*e.g.* Bishop *et al.*, 2008). Spectra were measured relative to Halon from 0.3 to 2.5 μm under ambient conditions with 5 nm spectral sampling. Infrared reflectance spectra were measured relative to a rough gold surface in a biconical configuration with 2 cm^{-1} spectral sampling from 1–50 μm in an environment purged of H_2O and CO_2 for 10–12 h. Composite, absolute reflectance spectra were prepared by scaling the FTIR data to the bidirectional data near 1.2 μm.

Emissivity measurements

TIR emissivity spectra of particulate and pellet samples were collected at the Mars Space Flight Facility at Arizona State University using a Nicolet Nexus 670 spectrometer configured to measure emitted energy (Christensen and Harrison, 1993; Ruff *et al.*, 1997). Samples were placed in copper sample cups painted black so that they behaved as a spectral blackbody, and were heated to 80ºC before and during the experiments to increase the signal-to-noise ratio. Spectra were scanned 240 times over the course of ~4 min, from 200 to 2000 cm^{-1} with 2 cm^{-1} spectral resolution. Blackbodies at 70 and 100ºC were measured to calibrate raw data to radiance (Christensen and Harrison, 1993). Radiance spectra were transformed to emissivity spectra by normalizing to the Planck curve corresponding to the sample temperature (Ruff *et al.*, 1997). Pellets were created by compressing ~0.2 g of particulate material to ~70 MPa (uncorrected for friction) in a hydraulic press for 3 min (Michalski *et al.*, 2005). Pellets were 1 cm in diameter and a few mm thick.

XRD-RH experiments

Powders for controlled-humidity powder XRD measurements were mounted as thin slurries on 'zero-background' quartz plates, which were mounted in an environmental chamber on a Bruker D8 powder diffractometer using CuKα radiation and an energy-dispersive Sol-X detector (Bruker, Karlsruhe, Germany). The use of thin slurry sample mounts allowed the powders to equilibrate quickly with the controlled-RH atmosphere. Relative humidity was controlled by an InstruQuest Inc. (Florida, USA) VGen RH generator. Diffraction measurements were made at 0 to 95% RH and back to 0% RH, in 10% RH steps to 90%, 5% steps from 90–95–90%, and 10% RH steps back to 0% RH. An initial equilibration time of 2 h was used at 0% RH, and a 1 h equilibration time was used before all other XRD measurements at each RH level. The XRD data were measured for allophane from 2 to 36º2θ and for imogolite from 2 to 18º2θ, counting for 2 s/0.02º step.

RESULTS

VNIR reflectance spectra

The VNIR reflectance spectra of allophane included bands near 1.4, 1.9, and 2.2 μm, plus a strong band that was nearly saturated from 2.7–3.5 μm (Figure 4a). For the spectra measured under ambient conditions where substantial adsorbed H_2O was present, the bands near 1.4 and 1.9 μm were much stronger and shifted toward longer wavelengths, as expected (*e.g.* Bishop *et al.*, 1994). The VNIR spectral properties of synthetic allophane and purified natural allophane were similar. The allophane-rich soil spectrum (Figure 4a) contained a weak broad band near 0.9–1 μm and an increasing slope from 0.4 to 0.6 μm compared to the pure allophane spectra. These additional features in the spectra of the untreated samples are consistent with the presence of iron and are typical of iron (oxyhydr)oxides (*e.g.* Morris *et al.*, 1985; Bishop and Murad, 1996). These features are also consistent with Fe(III)-bearing phyllosilicates (*e.g.* Bishop *et al.*, 1999, 2008), but no Fe_3OH bands were observed near 2.3 μm as are present in Fe(III)-bearing phyllosilicates and no evidence of phyllosilicates in the XRD patterns was noted. The synthetic Fe-bearing allophane contained similar features near 0.4–0.6 and 0.9–1 μm which are attributed to the Fe(III) shown to be present in isomorphic substitution for Al in the allophane structure through EXAFS experiments (Baker and Strawn, 2012). Note that in addition to the weak, broad Fe(III) band near 0.9–1.0 μm, an H_2O overtone centered at 0.97 μm was observed, which increased in intensity toward 1.0 μm in the spectra measured under hydrated conditions (dotted lines in Figure 4). This H_2O band was stronger in spectra of the synthetic samples than in spectra of the natural samples. The bands near 1.4, 1.9, and 2.2 μm were due to overtones and combinations of H_2O and OH in the structure and are described in more detail in a later section.

The VNIR reflectance spectra of imogolite also included bands near 1.4, 1.9, 2.2, and 2.7–3.5 μm (Figure 4b), and the 1.4 and 1.9 μm bands were again greatly intensified for spectra measured under ambient conditions where adsorbed H_2O contributes to the spectral features.

Mid-IR reflectance and emissivity spectra of fundamental vibrations

Reflectance (R) and emittance (E) both depend on the real (n) and imaginary (k) components of the index of

https://doi.org/10.1346/CCMN.2013.0610105 Published online by Cambridge University Press

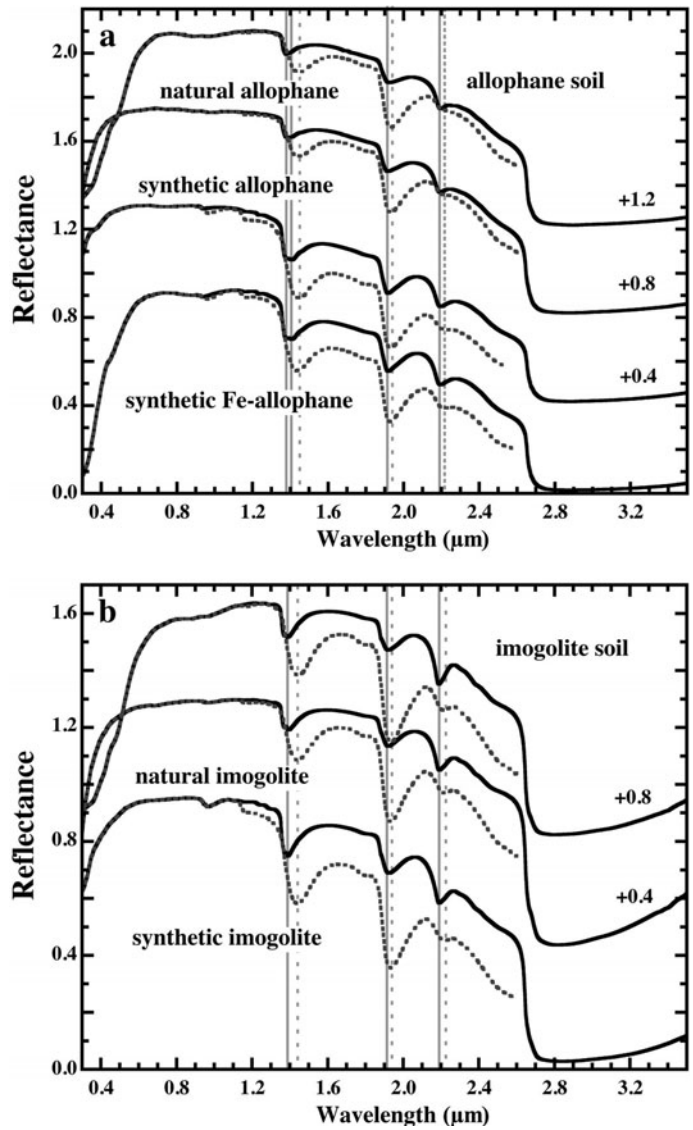

Figure 4. VNIR reflectance spectra of (a) allophane and (b) imogolite. Spectra are offset for clarity. Dashed lines refer to spectra measured under ambient RH conditions (0.3−2.5 μm). Solid lines refer to spectra measured under low-RH conditions (1−3.3 μm).

refraction and are, thus, influenced by surface scattering and particle size. They are related by Kirchhof's Law, where $R = 1-E$, which generally holds for Lambertian surfaces and larger grain sizes, although discrepancies are often noted for small particle sizes (Salisbury, 1993). Reflectance and emittance are both distinct from transmittance spectra, which only depend on k. H_2O bending vibrations were observed near 1650 cm^{-1} (~6.1 μm) for allophane (Figure 5a,b) and imogolite (Figure 5c,d). A strong single upward band (in inverse reflectance – note that this would be a downward band in reflectance) was observed for the synthetic allophane (Figure 5b) and synthetic imogolite (Figure 5d) spectra, whereas a weaker doublet feature was observed in the reflectance spectra of the natural samples (Figure 5a,c). These features indicated that additional hydrated phases were present in the natural samples and were not removed by the purification process. The spectral features at longer wavelengths were largely similar for the inverse reflectance spectra of loose powders and the emissivity spectra of pressed powders; however, the spectral bands were stronger for the spectra of the pressed powders, as expected (*e.g.* Michalski *et al.*, 2006).

Si–O stretching region

The Si−O−Al stretching vibrations occurred near 1010 cm^{-1} (9.9 μm) and 930 cm^{-1} (10.8 μm) in reflectance spectra of imogolite and near 1030 cm^{-1} (9.7 μm) and 940 cm^{-1} (10.6 μm) in reflectance spectra

https://doi.org/10.1346/CCMN.2013.0610105 Published online by Cambridge University Press

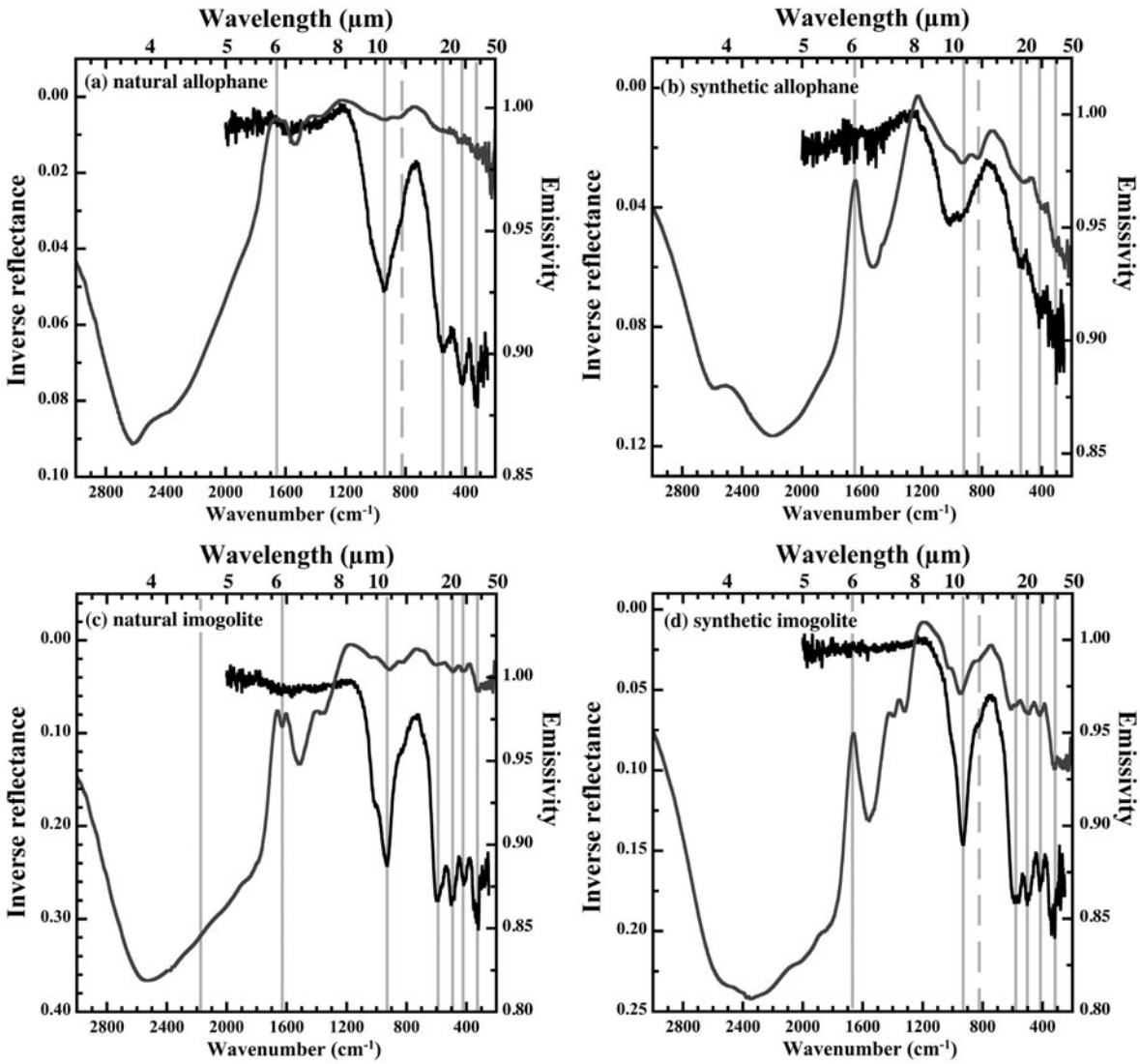

Figure 5. Mid-infrared reflectance and emissivity spectra from 200 to 3000 cm^{-1} (~3–50 μm) of (a) natural allophane, (b) synthetic allophane, (c) natural imogolite, and (d) synthetic imogolite.

of allophane (Figure 6). These are similar to the emissivity bands for Si–O stretching in high-silica aluminosilicate gel observed near 1070 cm^{-1} (9.3 μm) (*e.g.* Rampe *et al.*, 2012), near 1270 cm^{-1} (7.9 μm) and 1120 cm^{-1} (8.9 μm) for opal, and near 1130 cm^{-1} (8.8 μm) and 1045 cm^{-1} (9.6 μm) for Si–O–Al stretching in phyllosilicates (Michalski *et al.*, 2005; Bishop *et al.*, 2008). Rampe *et al.* (2012) observed a single band centered near 940 cm^{-1} in emissivity spectra of allophanes with low Si/Al ratios and a broad doublet feature near 1030 cm^{-1} and 940 cm^{-1} for allophanes with an Si/Al ratio of 0.92, similar to that observed for the natural allophane in the present study (Figure 6) which has an Si/Al ratio of 0.82. This doublet was shifted toward the 1030 cm^{-1} band in the synthetic sample (Figure 6), indicating that more Si–O–Si bonds were present. The Si–O–Al stretching band occurred near 985–995 cm^{-1} in transmittance spectra of allophane with high Si/Al ratios and near 962–970 cm^{-1} in transmittance spectra of allophane with low Si/Al ratios (Parfitt and Henmi, 1980; Henmi *et al.*, 1981). This band occurred as a doublet near 950–1000 cm^{-1} in transmittance spectra of imogolite and near 1000–1050 cm^{-1} in transmittance spectra of silica gel (Farmer *et al.*, 1979).

OH-bending region

OH-bending vibrations are generally observed from 590 cm^{-1} (16.9 μm) to 940 cm^{-1} (10.6 μm) in phyllosilicates (*e.g.* Farmer, 1974). A shoulder feature near 825 cm^{-1} (12.1 μm) was observed in reflectance

https://doi.org/10.1346/CCMN.2013.0610105 Published online by Cambridge University Press

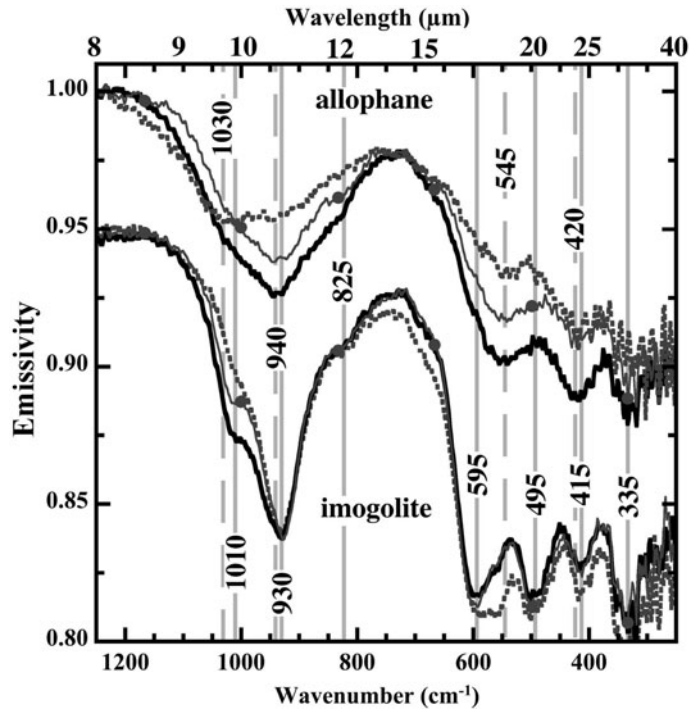

Figure 6. Emittance spectra from 1250–250 cm^{-1} (8–40 μm) showing the Si–O–Al stretching and bending vibrations. Spectra of the natural allophane and imogolite samples are shown in solid lines, spectra of the natural allophane and imogolite soils are shown with symbols, and spectra of the synthetic allophane and imogolite are shown in dashed lines. The imogolite spectra are offset by 0.05 on the vertical scale for clarity.

spectra of both allophane and imogolite and is attributed to in-plane Al–OH bending vibrations, based on this feature in phyllosilicates (*e.g.* Bishop *et al.*, 2002b). An additional band was observed at 595 cm^{-1} (16.8 μm) in imogolite spectra and a shoulder was present near 620 cm^{-1} (16.1 μm) in allophane spectra. These are more consistent with out-of-plane bending vibrations (*e.g.* Farmer, 1974) and are generally only observed in phyllosilicates when the structure is disrupted (*e.g.* Bishop *et al.*, 2002b). The features near 595 and 620 cm^{-1} could also be due to Al–O vibrations (Farmer, 1974). Bending vibrations for Si–OH in silica occur near 795 cm^{-1} (12.6 μm) and were observed only as a weak shoulder if at all in the allophane and imogolite spectra. This is consistent with the structural models (Figure 2) for allophane and imogolite that indicate a much greater abundance of OH bound to Al than to Si. Transmittance spectra of allophane and imogolite included a band near 690 cm^{-1} (Parfitt *et al.*, 1980; Parfitt and Henmi, 1980) that is probably related to the 595–620 cm^{-1} reflectance feature.

Si–O bending region

The bands near 545 cm^{-1} (18.3 μm) in the allophane spectra and near 495 cm^{-1} (20.2 μm) in the imogolite spectra (Figure 6) are attributed to Si–O–Al deformation, and the bands near 420 cm^{-1} (23.8 μm) in the allophane spectra and near 415 cm^{-1} (24.1 μm) in the imogolite spectra (Figure 6) are attributed to Si–O bending based on studies of phyllosilicate spectra (*e.g.* Farmer, 1974; Bishop *et al.*, 2002a; Michalski *et al.*, 2005). Related spectral bands are observed for Si–O bending vibrations for silica gel (near 440 cm^{-1}, 22.7 μm, Rampe *et al.*, 2012) and for opal (481 cm^{-1}, 20.8 μm, Bishop *et al.*, 2011). Shifts were not observed in the 545 and 420 cm^{-1} allophane bands with changing Si/Al ratio (Rampe *et al.*, 2012). Differences in these features for allophane and imogolite are attributed to the curvature of the structures as Si–O bending vibrations are probably sensitive to the position of neighboring atoms. An additional band was observed near 325–335 cm^{-1} (~30 μm) in emissivity and reflectance spectra of all allophane and imogolite samples. This also falls in the spectral region due to Si–O bending (Farmer, 1974) and was observed at 348 cm^{-1} in transmittance spectra of imogolite and allophane (Farmer *et al.*, 1977).

H_2O bending region

Single bands were observed in the H_2O bending region at 1645 cm^{-1} (6.08 μm) for reflectance spectra of synthetic allophane (Figure 7a) and 1662 cm^{-1} (6.02 μm) for synthetic imogolite (Figure 7b). Reflectance spectra of the natural samples exhibited doublets in this region: 1667 and 1606 cm^{-1} for allophane and 1662 and 1604 cm^{-1} for imogolite (Figure 7). A related band with variable width was

https://doi.org/10.1346/CCMN.2013.0610105 Published online by Cambridge University Press

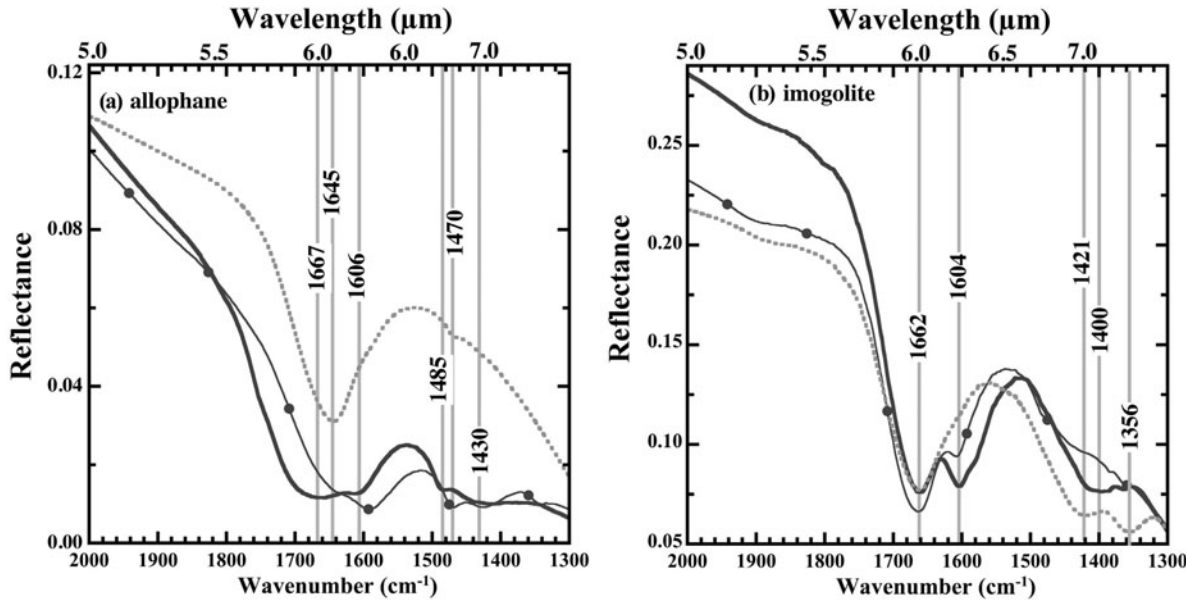

Figure 7. Reflectance spectra from 1300 to 2000 cm^{-1} (5−7.5 μm) of the H_2O bending region for (a) allophane and (b) imogolite. Spectra of the natural allophane and imogolite samples are shown in solid lines, spectra of the natural allophane and imogolite soils are shown with symbols, and spectra of the synthetic allophane and imogolite are shown in dashed lines. The natural allophane spectra were increased by a factor of two on the vertical scale for comparison with the synthetic spectrum.

observed in transmittance spectra of allophane and imogolite (Parfitt and Henmi, 1980). An additional feature was observed near 1400 cm^{-1} in reflectance spectra (Figure 7) and transmittance spectra (Parfitt and Henmi, 1980) of allophane and imogolite. A doublet was observed for the natural allophane (1485, 1430 cm^{-1}) and a single weak band was observed for the synthetic allophane (1470 cm^{-1}), whereas a doublet was observed for the synthetic imogolite (1421, 1356 cm^{-1}) and a single band was observed for the natural imogolite (1400 cm^{-1}). This band is attributed to OH bending vibrations of acid salts such as O_3SiOH groups that can be split into a doublet by resonance interactions (Ryskin, 1974). Alternatively, nitrates could be causing this feature near 1400 cm^{-1} (*e.g.* Pavia *et al.*, 1979). However, as a related feature has been observed in reflectance and transmittance spectra of some ferrihydrite samples, particularly natural samples containing Si (Bishop and Murad, 2002), the O_3SiOH interpretation may be more likely for these samples. Organic residues from the soil and/or Fe removal treatment could also be contributing to spectral features in this region. The band at 1356 cm^{-1} was probably due to organic admixtures. A sharper band was observed near 1380 cm^{-1} in transmittance spectra of the natural samples (not shown).

H_2O stretching region

A broad reflectance band was observed for both allophane and imogolite in the H_2O stretching region (Figure 8). This feature extended from ~3000−3700 cm^{-1} and is a composite of symmetric

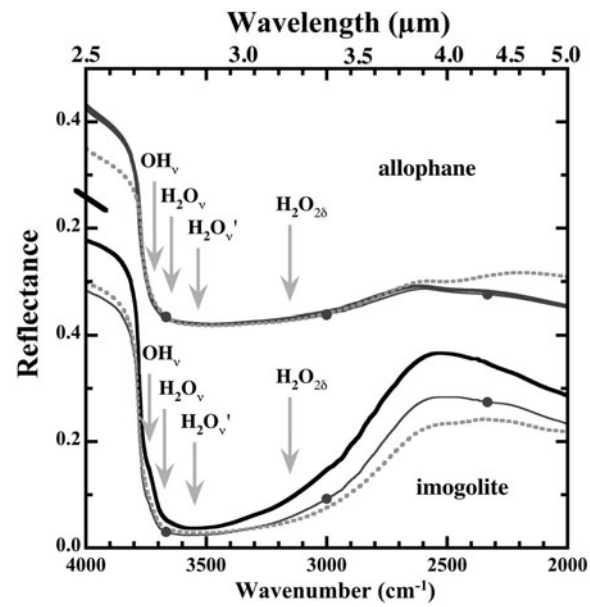

Figure 8. Reflectance spectra from 2000 to 4000 cm^{-1} (2.5−5 μm) of the OH and H_2O stretching region for allophane and imogolite. Spectra of the natural allophane and imogolite samples are shown in solid lines, the natural allophane and imogolite soils are shown with symbols, and the synthetic allophane and imogolite are shown in dashed lines. The positions of the features contributing to the broad band are marked as OH_v for OH stretching, H_2O_v for H_2O stretching, H_2O_v' for H_2O stretching at hydrated sites, and $H_2O_{2\delta}$ for bending overtones as described by Bishop *et al.* (1994).

https://doi.org/10.1346/CCMN.2013.0610105 Published online by Cambridge University Press

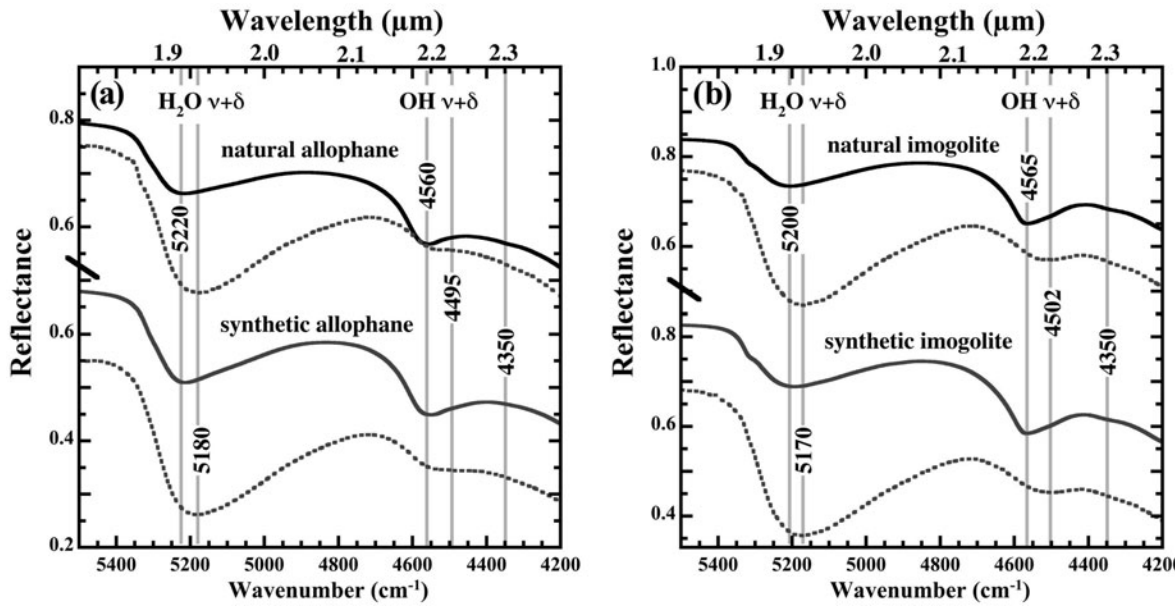

Figure 9. Reflectance spectra from 4200 to 5500 cm^{-1} (~1.8–2.4 μm) of the OH and H_2O combination band region for (a) allophane and (b) imogolite. Dashed lines refer to spectra measured under ambient RH conditions, whereas solid lines refer to spectra measured under low-RH conditions. ν+δ indicate the combination bending plus stretching vibration.

and asymmetric H_2O stretching vibrations, OH-stretching vibrations, and an overtone of the H_2O bending vibration as summarized for phyllosilicates (*e.g.* Bishop *et al.*, 1994). A broad, composite band was also observed in this region in transmittance spectra of allophane and imogolite (Parfitt and Henmi, 1980).

NIR reflectance spectra of combinations and overtones

OH combination band. An OH combination stretching plus bending band was observed at 4560 cm^{-1} (2.193 μm) for allophane (Figure 9a) and at 4565 cm^{-1} (2.191 μm) for imogolite (Figure 9b) measured under controlled, low-humidity conditions in reflectance spectra. These OH combination bands ($OH_{\nu+\delta}$) were broadened and shifted toward longer wavelengths, particularly in the case of imogolite for spectra measured under ambient (elevated RH) conditions (Figure 9). In reflectance spectra of phyllosilicates, these OH combination bands were not affected by humidity level and adsorbed H_2O molecules (*e.g.* Bishop *et al.*, 1994); however, this OH band in opal-A, opal-CT, and hydrated silica is dependent on adsorbed H_2O and H-bonding of the OH species (Anderson and Wickersheim, 1964). Thus, the OH bonds in allophane and imogolite are more similar in character to hydrated amorphous materials than to phyllosilicates.

H_2O combination band. The H_2O combination stretching plus bending band was observed at 5220 cm^{-1} (1.916 μm) for allophane (Figure 9a) and at 5200 cm^{-1} (1.923 μm) for imogolite (Figure 9b). Both of these bands were broad and asymmetric, similar to the H_2O stretching band shape. The magnitude of the H_2O combination band ($H_2O_{\nu+\delta}$) was greatly increased for spectra measured under ambient (elevated humidity) conditions, as expected. The band center was also shifted toward lower wavenumbers (longer wavelengths) due to the additional H-bonding as in the case of adsorbed H_2O in phyllosilicate spectra (Bishop *et al.*, 1994).

OH and H_2O overtones. Overtone bands of the fundamental stretching vibration were present for both OH and H_2O in allophane and imogolite spectra (Figure 10). A doublet occurred here due to the proximity of the OH overtone ($OH_{2\nu}$) and H_2O overtone ($H_2O_{2\nu}$). The $OH_{2\nu}$ occurred near 7263 cm^{-1} (1.377 μm) for allophane and near 7285–7305 cm^{-1} (1.369–1.373 μm) for imogolite, and the $H_2O_{2\nu}$ occurred near 7104–7139 cm^{-1} (1.401–1.407 μm) for allophane and near 7170–7205 cm^{-1} (1.388–1.395 μm) for imogolite. The exact positions of these overtone band centers varied among the natural and synthetic samples in the present study and probably depended on the Si/Al ratio and curvature of the structure. The $OH_{2\nu}$ band in phyllosilicates depends on the cation to which it relates. It shifts from near ~7000 cm^{-1} (1.42–1.43 μm) for Fe-smectite to ~7100 cm^{-1} (1.40–1.41 μm) for Al-smectite and to ~7200 cm^{-1} (1.38–1.39 μm) for Mg-smectite and also hydrated silica (*e.g.* Anderson and Wickersheim, 1964; Bishop *et al.*, 2002b, 2008). A broad H_2O stretching overtone band was also observed for adsorbed or outer-sphere H_2O in the allophane spectra near 6900 cm^{-1} (1.45 μm) (Figure 10a) and in the imogolite spectra near

https://doi.org/10.1346/CCMN.2013.0610105 Published online by Cambridge University Press

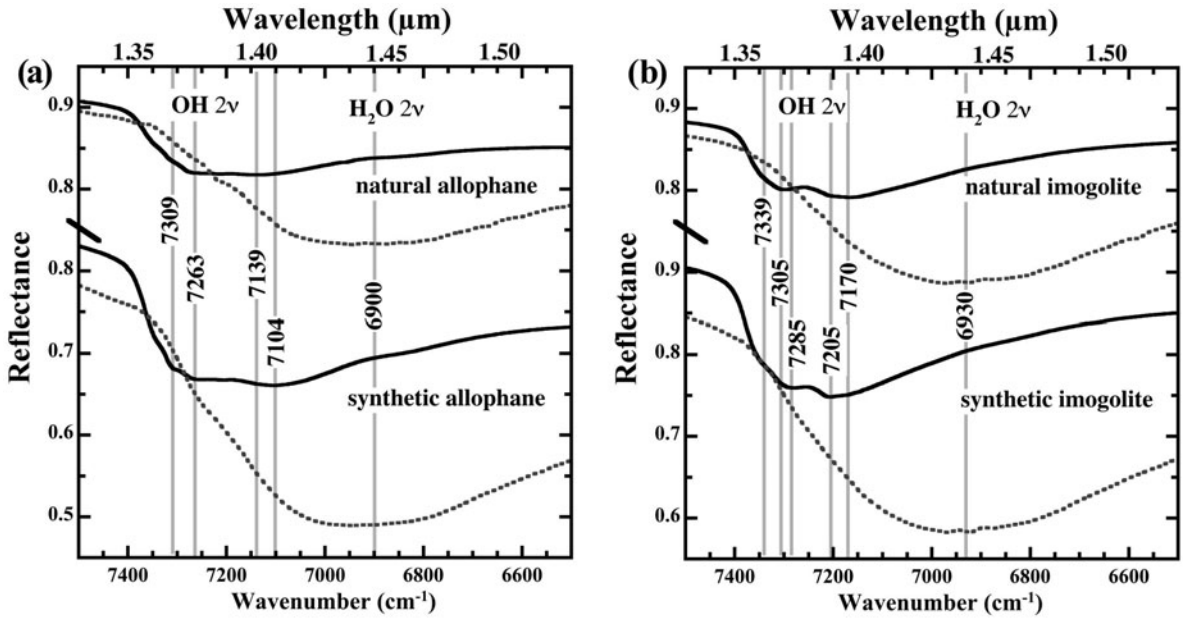

Figure 10. Reflectance spectra from 6500 to 7500 cm^{-1} (~1.3−1.55 μm) of the OH and H_2O stretching overtone (2ν) region for (a) allophane and (b) imogolite. Dashed lines refer to spectra measured under ambient RH conditions, whereas solid lines refer to spectra measured under low-RH conditions.

6930 cm^{-1} (1.44 μm) (Figure 10b). This band occurred for the samples measured under ambient (elevated humidity) conditions but was not observed for the samples measured under hydrated conditions.

XRD-RH experiments

The XRD data for imogolite (Figure 11) showed the expected strong, broad peak at 2−3º2θ, the broad maximum at ~5−7º2θ, and the weaker peak near 12º2θ consistent with the partially ordered structure (*e.g.* van der Gaast *et al.*, 1985). However, these data measured as a function of relative humidity (RH) revealed unexpected changes as a function of RH, with large decreases in low-angle scattering intensity with increasing RH. The low-angle scattering behavior of imogolite at 0 and 100% RH and at elevated temperatures was measured by van der Gaast *et al.* (1985), and their data (Figure 6 in van der Gaast *et al.*, 1985) showed a significant decrease in the intensity of low-angle scattering with increasing temperature, but they do not show the significant decrease in intensity of low-angle scattering observed under elevated RH conditions. In a study comparing XRD patterns of natural and synthetic imogolite, Farmer and Fraser (1979) noted shifts to larger *d* spacings or smaller 2θ values and attributed the sharp, low-angle peak to a hexagonal, close-packing array of the imogolite tubes. Although the positions of the broad maxima were unchanged in the present study, the intensity of the broad maximum from ~4 to 9º2θ decreased systematically from 0 to 95% RH and then

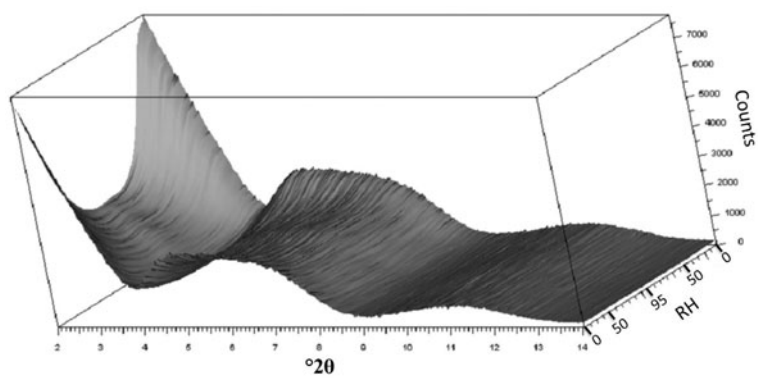

Figure 11. 3D representation of XRD data for the natural imogolite sample as the RH was increased from 0% to 95% and back to 0% (*z* axis). The low-angle (<9º2θ) intensity decreased at elevated RH levels. The XRD pattern is characteristic of imogolite.

https://doi.org/10.1346/CCMN.2013.0610105 Published online by Cambridge University Press

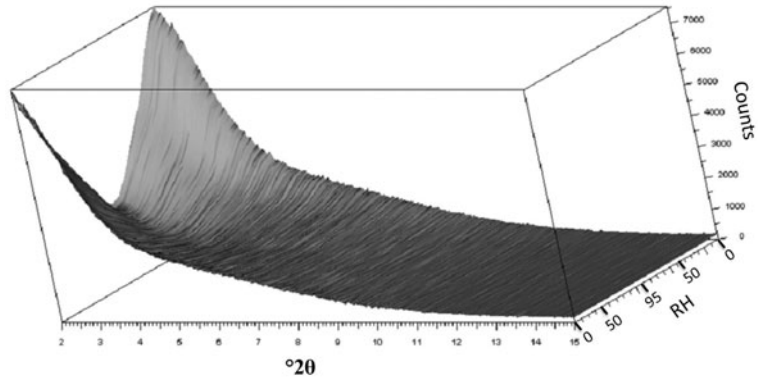

Figure 12. 3D representation of XRD data for the natural allophane sample as the RH was increased from 0% to 95% and back to 0% (*z* axis). The low-angle (<9º2θ) intensity decreased at elevated RH levels. This allophane exhibits no diffraction maxima, as expected.

increased again with a reduction in RH toward 0%. The low-angle scattered intensity changed in a similar manner. The broad maximum from ~9 to 14º2θ showed no significant change in intensity with RH. Such intensity changes are not common with well ordered, macrocrystalline materials, but they are similar to those observed with other poorly ordered materials such as opal-A and are probably related to adsorption of H_2O molecules onto the imogolite surface, as suggested by van der Gaast *et al.* (1985) for allophane.

The XRD data for allophane (Figure 12) showed a characteristic broad maximum near 3º2θ and a largely featureless diffraction pattern. Data measured as a function of RH showed large decreases in low-angle scattering intensity with increasing RH similar to those observed for imogolite (Figure 11). In the experiment with allophane, the present results were similar to a previous study (figure 1 in van der Gaast *et al.*, 1985) where the strong ~3º2θ peak observed under low-RH conditions disappeared under 100% RH. However, these results are different from those of Kaufhold *et al.* (2010) who measured the XRD pattern of an allophane-rich soil under variable RH conditions and observed little change in the scattering intensity. In that study, however, the XRD pattern appears to reflect the minor feldspar and quartz minerals rather than the allophane. In the present study, the low-angle peak at ~3º2θ decreased systematically from 0 to 95% RH and then increased again with a reduction in RH towards 0%. The character of the low-angle scattering changed significantly, with the greatest intensity increase at the lowest angles. As noted above, these intensity changes are not typically observed with well ordered materials, and are probably related to adsorption of H_2O molecules onto the allophane surface, as suggested by van der Gaast *et al.* (1985). Those authors postulated that the adsorption of H_2O molecules onto the allophane surfaces disrupted the regular packing of allophane pseudo-spherical particles. The present results for imogolite suggest the existence of a similar process in this tubular material.

DISCUSSION

Band assignments were made for allophane and imogolite based on the results of the present study of reflectance and emissivity spectra and previous studies of transmittance spectra (*e.g.* Farmer *et al.*, 1977, 1979, 1983; Parfitt and Henmi, 1980; Parfitt *et al.*, 1980; Henmi *et al.*, 1981). These are expressed in both frequency (wavenumber) and wavelength units (cm^{-1} and μm, respectively) for allophane (Table 1) and imogolite (Table 2) in order to facilitate usage in both the fields of chemistry and geology. The band centers for the OH and H_2O bands were used to compare calculated

Table 1. Band assignments for spectral features observed for allophane.

Wavenumber (cm^{-1})	Wavelength (μm)	Feature
7263	1.377	$OH_{2\nu}$
7104–7139	1.401–1.407	$OH_{2\nu}$
6900	1.45	$H_2O_{2\nu}$
5220	1.916	$H_2O_{\nu+\delta}$
4560	2.193	$OH_{\nu+\delta}$
4495	2.225	$OH_{\nu+\delta}$
~3640–3740	~2.67–2.74	OH_{ν}
~3500–3600	~2.78–2.86	H_2O_{ν}
~3120–3165	~3.2	$H_2O_{2\delta}$
1606–1667	6.00–6.23	H_2O_{δ}
1430–1485	6.73–6.99	OH_{δ} for O_3SiOH
1030	9.7	$Si–O–Al_{\nu}$
940	10.6	$Si–O–Al_{\nu}$
825	12.1	OH_{δ}
610	16.4	out–of-plane OH_{δ}
545	18.3	$Si\text{-}O\text{-}Al_{\delta}$
420	23.8	$Si–O_{\delta}$
335	29.9	$Si–O_{\delta}$

ν indicates stretching vibration; δ indicates bending vibration; band assignments are based on the present study and on previous transmission IR studies (*e.g.* Farmer *et al.*, 1977; Parfitt *et al.*, 1980; Henmi *et al.*, 1981).

https://doi.org/10.1346/CCMN.2013.0610105 Published online by Cambridge University Press

Table 2. Band assignments for spectral features observed for imogolite.

Wavenumber (cm^{-1})	Wavelength (μm)	Feature
7285–7305	1.369–1.373	$OH_{2\nu}$
7170–7205	1.388–1.394	$OH_{2\nu}$
6930	1.44	$H_2O_{2\nu}$
5200	1.923	$H_2O_{\nu+\delta}$
4565	2.191	$OH_{\nu+\delta}$
4502	2.221	$OH_{\nu+\delta}$
3700		OH_{ν}
~3670–3755	~2.66–2.72	OH_{ν}
~3500–3600	~2.78–2.86	H_2O_{ν}
~3150	~3.2	$H_2O_{2\delta}$
1604–1662	6.02–6.23	H_2O_{δ}
~1400–1421	7.14–7.37	OH bend for O_3SiOH
1010	9.9	$Si–O–Al_{\nu}$
930	10.8	$Si–O–Al_{\nu}$
825	12.1	OH_{δ}
595	16.8	out-of-plane OH_{δ}
495	20.2	$Si–O–Al_{\delta}$
415	24.1	$Si–O_{\delta}$
335	29.9	$Si–O_{\delta}$

ν indicates stretching vibration; δ indicates bending vibration; band assignments are based on the present study and on previous transmission IR studies (*e.g.* Farmer *et al.*, 1977; Parfitt *et al.*, 1980; Henmi *et al.*, 1981).

and measured frequencies of the combination bands and overtones in relation to the fundamental vibrations (Tables 3 and 4) as in previous studies (Bishop *et al.*, 2002a; Petit *et al.*, 2004).

The frequency of the $OH_{\nu+\delta}$ combination band should equal the sum of the frequencies of the OH_{ν} and OH_{δ} bands. The OH_{ν} band is difficult to resolve in reflectance spectra because of the multiple, overlapping vibrations near 3300–3760 cm^{-1} (~2.7–3.0 μm) due to a distribution of H_2O_{ν} and $H_2O_{2\delta}$ bands. The frequencies of the OH_{ν} vibration for allophane and imogolite were estimated by subtracting the OH_{δ} frequency from the $OH_{\nu+\delta}$ frequency as in Bishop *et al.* (2002a) for phyllosilicates. The OH_{ν} frequency was also estimated from the $OH_{2\nu}$ frequency using the equation $F_{2\nu} = 2\ (F_{\nu}) - 171.27$, where F is frequency (cm^{-1}), as in Petit *et al.* (2004) for phyllosilicates. Good agreement was found using these two methods, lending support to the band assignments. Two sets of OH_{ν} vibrations were found for allophane and imogolite (Table 3b). The OH_{ν} vibrations were estimated at 3638–3670 cm^{-1} (2.72–2.75 μm) and 3717–3740 cm^{-1} (2.67–2.69 μm) for allophane and at 3671–3688 cm^{-1} (2.71–2.72 μm) and 3728–3755 cm^{-1} (2.66–2.68 μm) for imogolite. For both allophane and imogolite, a doublet was present for the $OH_{2\nu}$. The lower-frequency vibration was shown to be due to $OH_{2\nu}$ rather than $H_2O_{2\nu}$ as the derived OH_{ν} frequency is comparable to the OH_{ν} frequency derived from a shoulder on the $OH_{\nu+\delta}$ band and the OH_{δ} band. A very weak band was observed near 4350 cm^{-1} (2.30 μm) for both allophane and imogolite ($OH_{\nu+\delta}$ (2), Table 3a). This band assignment was tested by calculating OH_{ν} from this and the potential OH_{δ} (2) band at 595–610 cm^{-1} (Table 3b). The agreement of this OH_{ν} with that determined from the overtone is within 25 cm^{-1}, which suggests that the 610 cm^{-1} band in allophane spectra and the 595 cm^{-1} band in imogolite spectra are indeed due to OH-bending vibrations and not to Al–O vibrations.

The frequency of the H_2O_{ν} vibration was estimated in a similar manner to that of the OH_{ν}, using the measured

Table 3a. Measured band centers for OH vibrations.

	$OH_{2\nu}$	$OH_{2\nu}$*	$OH_{\nu+\delta}$ (1)	$OH_{\nu+\delta}$ (1)*	$OH_{\nu+\delta}$ (2)	OH_{δ} (1)	OH_{δ} (2)
Allophane natural	7263	7139	4560	4495	4350	825	610
Allophane synthetic	7263	7104	4560	4495	4350	825	610
Imogolite natural	7305	7170	4565	4502	4350	825	595
Imogolite synthetic	7285	7205	4565	4502	4350	825	595

ν indicates stretching vibration; δ indicates bending vibration; * indicates estimated band based on shoulder.

Table 3b. Calculated band centers for OH vibrations.

	OH_{ν} calc. from $OH_{2\nu}$	OH_{ν} * calc. from $OH_{2\nu}$	OH_{ν} (1) calc. from $OH_{\nu+\delta}$ (1)	OH_{ν} (1)* calc. from $OH_{\nu+\delta}$ (1)*	OH_{ν} (2) calc. from $OH_{\nu+\delta}$ (2)
Allophane natural	3717	3655	3735	3670	3740
Allophane synthetic	3717	3638	3735	3670	3740
Imogolite natural	3738	3671	3740	3677	3755
Imogolite synthetic	3728	3688	3740	3677	3755

ν indicates stretching vibration; δ indicates bending vibration; * indicates estimated band based on shoulder.

https://doi.org/10.1346/CCMN.2013.0610105 Published online by Cambridge University Press

Table 4. Measured and calculated band centers for H_2O vibrations.

	H_2O_ν calc. from $H_2O_{2\nu}$	H_2O_ν calc. from $H_2O_{\nu+\delta}$	$H_2O_{2\delta}(1)$ calc. from $H_2O_\delta(1)$	$H_2O_{2\delta}(2)$ calc. from H_2O_δ (2)	$H_2O_{2\nu}'$ meas.	$H_2O_{\nu+\delta}$ meas.	$H_2O_\delta(1)$ meas.	H_2O_δ (2) meas.
Allophane natural	3536	3553	3163	3041	6900	5220	1667	1606
Allophane synthetic	3536	3575	3119		6900	5220	1645	
Imogolite natural	3551	3538	3153	3037	6930	5200	1662	1604
Imogolite synthetic	3551	3538	3153		6930	5200	1662	

Calc. is calculated band centers; meas. is measured band centers; ν indicates stretching vibration; δ indicates bending vibration; ′ indicates band that appeared under ambient (hydrated) conditions.

combination and overtone frequencies (Table 4). The $H_2O_{2\nu}$ vibration was greatly enhanced in the ambient spectra that were measured under higher humidity conditions, but was very weak in the low-RH spectra. The H_2O_ν frequencies calculated from this overtone were close to the H_2O_ν values determined from the measured frequencies of the clearly observed $H_2O_{\nu+\delta}$ and H_2O_δ bands (Tables 1 and 2). This supports the assignment of the $H_2O_{2\nu}$ frequency near 6900−6930 cm^{-1} (1.44−1.45 μm) for allophane and imogolite, rather than at higher wavenumbers where the $OH_{2\nu}$ vibration is located.

The significant differences observed for the H_2O bands in spectra measured under different RH conditions and the marked changes in XRD intensity with changing RH conditions indicate that both allophane and imogolite readily adsorb H_2O molecules onto their surfaces and that this additional H_2O affects their structures. The XRD intensity near 4−9°2θ for smectites increased with increasing RH, the opposite of what was observed for allophane and imogolite (Figures 11−12). The adsorption of H_2O molecules at high relative humidity was suggested by van der Gaast *et al.* (1985) to disrupt the regular packing of allophane spheres, thereby disrupting the semi-regular arrangement and decreasing the low-angle scattering. Although van der Gaast *et al.* (1985) did not see a significant decrease in low-angle scattering intensity with humidity for imogolite, the present results suggest that a process similar to that of allophane also operates for imogolite. Additional low-angle scattering studies are needed to fully understand the XRD results.

The spectral signatures for the allophane-rich soil and purified allophane sample, as well as the imogolite-rich soil and the purified imogolite sample, were, in general, quite similar. This bodes well for remote detection of allophane and imogolite. The presence of ferric oxide-bearing phases contributes an increased slope to the spectra from 0.4−0.6 μm and adds a weak band near 0.9 μm (Figure 4). Ferric oxide-bearing phases have been observed in other studies of natural allophane-rich soils (*e.g.* Kaufhold *et al.*, 2010) and may be commonly present in these materials. Further, the Kaufhold *et al.* (2010) study suggested that some of the Fe is present in the allophane structure, supporting the need for additional analysis of synthetic Fe-bearing allophanes (*e.g.* Baker and Strawn, 2012) to better understand this phase. The spectral signatures in the TIR region (Figure 6) are also largely unchanged for the soils and purified samples. The spectral region that is affected the most is from 1300−1800 cm^{-1} (5.6−7.7 μm) and may include contributions from organic admixtures. Changes were observed in the H_2O bending doublet near 1604−1667 cm^{-1} (6.0−6.2 μm) and in the OH-bending doublet attributed to O_3SiOH near 1400−1485 cm^{-1} (~7.1–7.4 μm). The doublets for both of these features tended to be shifted or less well resolved for spectra of the soils compared to spectra of the purified samples. Differences were also noted for these features in spectra of the natural and synthetic allophanes and imogolites, which suggest that these bands are less well defined for these samples than the spectral features in the VNIR and TIR regions more commonly used in remote-sensing studies.

SUMMARY AND CONCLUSIONS

This study of the spectral and hydration properties of allophane and imogolite builds on the results of many earlier studies to produce reflectance and emissivity spectra needed for remote-sensing detection of these minerals. As imogolite and allophane are generally indicators of geochemical conditions different from phyllosilicates such as smectite and halloysite, identification of imogolite and allophane should enable a more complete view of the geochemical environment during formation. Both natural and synthetic samples were studied here in order to observe which spectral features are constant and which are variable, depending on minor differences in Si/Al ratio, hydration state, and other mineral parameters. The spectra of allophane-rich soil and imogolite-rich soil were also compared with the spectra of the purified samples in order to evaluate which spectral features could be changed or masked in natural environments. The diagnostic VNIR and TIR features for allophane and imogolite are mostly unchanged in the spectra of the soil and the natural

https://doi.org/10.1346/CCMN.2013.0610105 Published online by Cambridge University Press

and synthetic samples. However, the spectral features in the range 1300–1800 cm^{-1} (5.6–7.7 μm) exhibited variations among the soil and the natural and synthetic samples that make the features due to H_2O_δ and OH_δ in O_3SiOH less useful for remote-sensing studies of allophane and imogolite.

Allophane and imogolite spectral properties are sufficiently different from each other and related clay minerals and hydrated silica components to allow for their identification using remote sensing. However, a wide distribution in structure and composition exists among allophane and imogolite types, and samples at the borders of these groups will, therefore, be more difficult to discriminate. Allophane can be identified in the NIR region using the OH overtone doublet at 1.38 and 1.40 μm, the H_2O combination band at 1.92 μm, and the OH combination band at 2.19 μm. The doublet occurs at 1.37 and 1.39 μm for imogolite. The OH overtone doublet and combination band in spectra of allophane and imogolite occur at shorter wavelengths compared to these features in spectra of other aluminosilicates and opaline silica. The H_2O combination band occurs at longer wavelengths for allophane and imogolite spectra. The OH combination band for allophane and imogolite is broader than that observed for smectites but narrower than that observed for opaline silica. The combination of these spectral parameters should enable identification and discrimination of allophane and imogolite from other aluminosilicates in reflectance spectroscopy investigations. As bands are observed near 1.4, 1.9, and 2.2 μm for many AlOH- and SiOH-bearing minerals, remote-sensing studies involving two or more of these features will be able to more accurately identify and distinguish allophane and imogolite from other aluminosilicates. The TIR region spectra of allophane and imogolite exhibit striking differences in the Si–O–Al stretching and bending vibrations compared with those in other aluminosilicates and opaline silica. The Si–O–Al stretching bands near 1030 and 940 cm^{-1} (~9.7 and 10.6 μm) and the Si–O–Al bending bands near 545 and 420 cm^{-1} (~18 and 24 μm) in spectra of allophane are shifted sufficiently from the Si–O–Al stretching bands near 1010 and 930 cm^{-1} (~9.9 and 10.7 μm) and the Si–O–Al bending bands near 495 and 415 cm^{-1} (~20 and 24 μm) in spectra of imogolite to distinguish these samples in emissivity spectra. The Si–O–Al stretching and bending bands for allophane and imogolite are shifted greatly from those of other aluminosilicates and opaline silica and should enable unique detections of these phases in emission spectroscopy studies.

ACKNOWLEDGMENTS

Thanks are extended to C. Pieters, T. Hiroi, and NASA's PGG program and the NISLI for the reflectance spectra collected at Brown University's RELAB facility and to P. Christensen and the Mars Space Flight Facility at Arizona State University for the use of the thermal emission spectrometer facility. The authors are grateful to S. Petit, J. Stucki, and two anonymous reviewers for helpful comments that improved the manuscript. This work was supported by NASA's Mars Fundamental Research program and the NASA Postdoctoral Program.

REFERENCES

Abidin, A., Matsue, N., and Henmi, T. (2007a) Differential formation of allophane and imogolite: Experimental and molecular orbital study. *Journal of Computer-Aided Materials Design*, **14**, 5–18.

Abidin, Z., Matsue, N., and Henmi, T. (2007b) Nanometer-scaled chemical modification of nano-ball allophane. *Clays and Clay Mineral*, **55**, 443–449.

Abidin, Z., Matsue, N., and Henmi, T. (2008) A new method for nano-tube imogolite synthesis. *Japanese Journal of Applied Physics*, **47**, 5079–5082.

Abidin, Z., Matsue, N., and Henmi, T. (2009) Validity of the new method for imogolite synthesis and its genetic implication. Pp. 331–341 in: *Interdisciplinary Studies on Environmental Chemistry – Environmental Research in Asia* (Y. Obayashi, T. Isobe, A. Subramanian, S. Suzuki, and S. Tanabe, editors). TERRAPUB.

Alvarez-Ramirez, F. (2007) Ab initio simulation of the structural and electronic properties of aluminosilicate and aluminogermanate natotubes with imogolite-like structure, *Physical Review B*, **76**, 125421.

Anderson, J.H. and Wickersheim, K.A. (1964) Near infrared characterization of water and hydroxyl groups on silica surfaces. *Surface Science*, **2**, 252–260.

Baker, L. and Strawn, D. (2012) Fe K-edge XAFS spectra of phyllosilicates of varying crystallinity. *Physics and Chemistry of Minerals*, **39**, 675–684.

Bish, D.L., Wu, W., Carey, J.W., Costanzo, P., Giese, R.F., Earl, W., and van Oss, C.J. (1999) Effects of steam on the surface properties of Na-smectite. Pp. 569–575 in: *Clays for Our Future* (H. Kodama, A.R. Mermut, and J.K. Torrance, editors). Proceedings of the 11th Annual International Clay Conference, Ottawa, Canada, 1997. ICC97 Organizing Committee.

Bishop, J.L. and Murad, E. (1996) Schwertmannite on Mars? Spectroscopic analyses of schwertmannite, its relationship to other ferric minerals, and its possible presence in the surface material on Mars. Pp. 337–358: *Mineral Spectroscopy: A tribute to Roger G. Burns*. (M.D. Dyar, C. McCammon, and M.W. Schaefer, editors). The Geochemical Society, St. Louis, Missouri, USA.

Bishop, J.L. and Murad, E. (2002) Spectroscopic and geochemical analyses of ferrihydrite from hydrothermal springs in Iceland and applications to Mars. Pp. 357–370 in: *Volcano–Ice Interactions on Earth and Mars* (J.L. Smellie and M.G. Chapman, editors). Special Publication No. **202**, Geological Society, London.

Bishop, J.L., Pieters, C.M., and Edwards, J.O. (1994) Infrared spectroscopic analyses on the nature of water in montmorillonite. *Clays and Clay Minerals*, **42**, 701–715.

Bishop, J.L., Murad, E., Madejová, J., Komadel, P., Wagner, U., and Scheinost, A. (1999) Visible, Mössbauer and infrared spectroscopy of dioctahedral smectites: Structural analyses of the Fe-bearing smectites Sampor, SWy-1 and SWa-1. Pp. 413–419 in: *11th International Clay Conference, June, 1997* (H. Kodama, A.R. Mermut, and J.K. Torrance, editors).

Bishop, J.L., Madeová, J., Komadel, P., and Fröschl, H. (2002a) The influence of structural Fe, Al and Mg on the infrared OH bands in spectra of dioctahedral smectites. *Clay Minerals*, **37**, 607–616.

Bishop, J.L., Murad, E., and Dyar, M.D. (2002b) The influence

of octahedral and tetrahedral cation substitution on the structure of smectites and serpentines as observed through infrared spectroscopy. *Clay Minerals*, **37**, 617–628.

Bishop, J.L., Lane, M.D., Dyar, M.D., and Brown, A.J. (2008) Reflectance and emission spectroscopy study of four groups of phyllosilicates: Smectites, kaolinite-serpentines, chlorites and micas. *Clay Minerals*, **43**, 35–54.

Bishop, J.L., Gates, W.P., Makarewicz, H.D., McKeown, N.K., and Hiroi, T. (2011) Reflectance spectroscopy of beidellites and their importance for Mars. *Clays and Clay Minerals*, **59**, 376–397.

Buurman, P. and van Reeuwijk, L.P. (1984) Proto-imogolite and the process of podzol formation: a critical note. *Journal of Soil Science*, **35**, 447–452.

Chipera, S.J., Carey, J.W., and Bish, D.L. (1997) Controlled-humidity XRD analyses: Application to the study of smectite expansion/contraction. Pp. 713–722 in: *Advances in X-ray Analysis* (J.V. Gilfrich, I.C. Noyan, R. Jenkins, T.C. Huang, R.L. Snyder, D.K. Smith, M.A. Zaitz, and P.K. Predecki, editors). Plenum Press, New York.

Christensen, P.R. and Harrison, S.T. (1993) Thermal infrared emission spectroscopy of natural surfaces: Application to desert varnish coatings on rocks. *Journal of Geophysical Research*, **98**, 19,819–19,834.

Cradwick, P.D.G., Farmer, V.C., Russell, J.D., Masson, C.R., Wada, K., and Yoshinaga, N. (1972) Imogolite, a hydrated aluminium silicate of tubular structure. *Nature Physical Science*, **240**, 187–189.

Creton, B., Bougeard, D., Smirnov, K.S., Guilment, J., and Poncelet, O. (2008a) Structural model and computer modeling study of allophane. *The Journal of Physical Chemistry C*, **112**, 358–364.

Creton, B., Bougeard, D., Smirnov, K.S., Guilment, J., and Poncelet, O. (2008b) Molecular dynamics study of hydrated imogolite. 1. Vibrational dynamics of the nanotube. *The Journal of Physical Chemistry C*, **112**, 10013–10020.

Demichelis, R., Noel, Y., D'Arco, P., Maschio, L., Orlando, R., and Dovesi, R. (2010) Structure and energetics of imogolite: a quantum mechanical ab initio study with B3LYP hybrid functional. *Journal of Materials Chemistry*, **20**, 10417–10425.

Farmer, V.C. (1974) The layer silicates. Pp. 331–363 in: *The Infrared Spectra of Minerals* (V.C. Farmer, editor). Monograph **4**, The Mineralogical Society, London.

Farmer, V.C. and Fraser, A.R. (1979) Synthetic Imogolite, a Tubular Hydroxyaluminium Silicate. Pp. 547–553 in: *Proceedings of the VI International Clay Conference, Oxford, UK* (M.M. Mortland and V.C. Farmer, editors). Developments in Sedimentology, **27**. Elsevier, Amsterdam.

Farmer, V.C., Fraser, A.R., and Tait, J.M. (1977) Synthesis of imogolite: a tubular aluminum silicate polymer. *Journal of the Chemical Society, Clinical Communications*, **12**, 462–463.

Farmer, V.C., Fraser, A.R., and Tait, J.M. (1979) Characterization of the chemical structures of natural and synthetic aluminosilicate gels and sols by infrared spectroscopy. *Geochimica et Cosmochimica Acta*, **43**, 1417–1420.

Farmer, V.C., Adams, M.J., Fraser, A.R., and Palmieri, F. (1983) Synthetic imogolite: properties, synthesis, and possible applications. *Clay Minerals*, **18**, 459–472.

Fieldes, M. (1955) Clay mineralogy of New Zealand soils, Part II: Allophane and related mineral colloids. *New Zealand Journal of Science and Technology*, **B37**, 336–350.

Guimarães, L., Enyashin, A.N., Frenzel, J., Heine, T., Duarte, H.A., and Seifert, G. (2007) Imogolite nanotubes: stability, electronic, and mechanical properties. *ACS Nano*, **1**, 362–368.

Gustafsson, J.P., Karltun, E., and Bhattacharya, P. (1998) *Allophane and imogolite in Swedish Soils.* Division of Land and Water Resources, Department of Civil and Environmental Engineering, Sweden, 33 pp.

Henmi, T. (1980) Effect of SiO_2/Al_2O_3 ratio on the thermal reactions of allophane. *Clays and Clay Minerals*, **28**, 92–96.

Henmi, T. and Huang, P.M. (1987) Effect of phosphate on the formation of imogolite. *Proceedings of the International Clay Conference 1985, Denver* (L.G. Schultz, H. van Olphen, and F.A. Mumpton, editors). The Clay Minerals Society, pp. 231–236.

Henmi, T. and Wada, K. (1976) Morphology and composition of allophane. *American Mineralogist*, **61**, 379–390.

Henmi, T., Tange, K., Minagawa, T., and Yoshinaga, N. (1981) Effect of SiO_2/Al_2O_3 ratio on the thermal reactions of allophane. II. Infrared and X-ray powder diffraction data. *Clays and Clay Minerals*, **29**, 124–128.

Kaufhold, S., Kaufhold, A., Jahn, R., Brito, S., Dohrmann, R., Hoffmann, R., Gliemann, H., Weidler, P., and Frechen, M. (2009) A new massive deposit of allophane raw material in Ecuador. *Clays and Clay Minerals*, **57**, 72–81.

Kaufhold, S., Ufer, K., Kaufhold, A., Stucki, J.W., Anastácio, A.S., Jahn, R., and Dohrmann, R. (2010) Quantification of allophane from Ecuador. *Clays and Clay Minerals*, **58**, 707–716.

Kodama, H. and Wang, C. (1989) Distribution and characterization of noncrystalline inorganic components in Spodosols and Spodosol-like soils. *Soil Science Society of America Journal*, **53**, 526–534.

Konduri, S., Mukherjee, S. and Nair, S. (2006) Strain energy minimum and vibrational properties of single-walled aluminosilicate nanotubes. *Physical Review B*, **74**, 033401.

Lundström, U.S., Van Breemen, N., and Bain, D.C. (2000) The podzolization process. A review. *Geoderma*, **94**, 91–107.

MacKenzie, K.J.D., Bowden, M.E., Brown, W.M., and Meinhold, R.H. (1989) Structure and thermal transformations of imogolite studied by ^{29}Si and ^{27}Al high-resolution solid-state nuclear magnetic resonance. *Clays and Clay Minerals*, **37**, 317–324.

Mehra, O.P. and Jackson, M.L. (1960) Iron oxide removal from soils and clays by a dithionite-citrate system buffered with sodium bicarbonate. *Clays and Clay Minerals*, **7**, 317–327.

Michalski, J.R., Kraft, M.D., Sharp, T.G., Williams, L.B., and Christensen, P.R. (2005) Mineralogical constraints on the high-silica Martian surface component observed by TES. *Icarus*, **174**, 161–177.

Michalski, J.R., Kraft, M.D., Sharp, T.G., Williams, L.B., and Christensen, P.R. (2006) Emission spectroscopy of clay minerals and evidence for poorly crystalline aluminosilicates on Mars from Thermal Emission Spectrometer data. *Journal of Geophysical Research*, **111**, E03004, doi:10.1029/2005JE002438.

Montarges-Pelletier, E., Bogenez, S., Pelletier, M., Razafitianamaharavo, A., Ghanbaja, J., Lartiges, B., and Michot, L. (2005) Synthetic allophane-like particles: textural properties. *Colloids and Surfaces A: Physicochemical and Engineering Aspects*, **255**, 1–10.

Morris, R.V., Lauer Jr., H.V., Lawson, C.A., Gibson Jr., E.K., Nace, G.A., and Stewart, C. (1985) Spectral and other physicochemical properties of submicron powders of hematite (α-Fe_2O_3), maghemite (γ-Fe_2O_3), magnetite (Fe_3O_4), goethite (α-FeOOH), and lepidocrocite (γ-FeOOH). *Journal of Geophysical Research*, **90**, 3126–3144.

Nagasawa, K. (1978) Weathering of volcanic ash and pyroclastic materials. Pp. 105–125 in: *Clays and Clay Minerals of Japan* (T. Sudo and S. Shimoda, editors). Developments in Sedimentology. Kodansha, Japan and Elsevier, Amsterdam.

Ndayiragije, S. and Delvaux, B. (2003) Coexistence of allophane, gibbsite, kaolinite and hydroxy-Al-interlayered

2:1 clay minerals in a perudic Andosol. *Geoderma*, **117**, 203–214.
Parfitt, R. (1990) Allophane in New Zealand – a review. *Soil Research*, **28**, 343–360.
Parfitt, R.L. (2009) Allophane and imogolite: role in soil biogeochemical processes. *Clay Minerals*, **44**, 135–155.
Parfitt, R.L. and Henmi, T. (1980) Structure of some allophanes from New Zealand. *Clays and Clay Minerals*, **28**, 285–294.
Parfitt, R.L., Furkert, R.J., and Henmi, T. (1980) Identification and structure of two types of allophane from volcanic ash soils and tephra. *Clays and Clay Minerals*, **28**, 328–334.
Parfitt, R.L., Childs, C.W., and Eden, D.N. (1988) Ferrihydrite and allophane in four andepts from Hawaii and implications for their classification. *Geoderma*, **41**, 223–241.
Pavia, D.L., Lampman, G.M., and Kriz, G.S. (1979) *Introduction to Spectroscopy: A Guide for Students of Organic Chemistry*. Saunders College, Philadelphia, USA.
Petit, S., Decarreau, A., Martin, F., and Buchet, R. (2004) Refined relationship between the position of the fundamental OH stretching and the first overtones for clays. *Physics and Chemistry of Minerals*, **31**, 585–592.
Rampe, E.B., Kraft, M.D., Sharp, T.G., Golden, D.C., Ming, D.W., and Christensen, P.R. (2012) Allophane detection on Mars with Thermal Emission Spectrometer data and implications for regional-scale chemical weathering processes. *Geology*, **40**, 995–998.
Ruff, S.W., Christensen, P.R., Barbera, P.W., and Anderson, D.L. (1997) Quantitative thermal emission spectroscopy of minerals: A technique for measurement and calibration. *Journal of Geophysical Research*, **102**, 14,899–14,913.
Russell, J.D., McHardy, W.J., and Fraser, A.R. (1969) Imogolite: A unique aluminosilicate. *Clay Minerals*, **8**, 87–99.
Ryskin, Y.I. (1974) The vibrations of protons in minerals: Hydroxyl, water and ammonium. Pp. 137–181 in: *The Infrared Spectra of Minerals* (V.C. Farmer, editor). Monograph **4**, The Mineralogical Society, London.
Saalfeld, H. and Wedde, M. (1974) Refinement of the crystal structure of gibbsite, $Al(OH)_3$. *Zeitschrift für Kristallographie*, **139**, 129–135.
Salisbury, J.W. (1993) Mid-infrared spectroscopy: Laboratory data. Pp. 79–98 in: *Remote Geochemical Analysis: Elemental and Mineralogical Composition* (C.M. Pieters and P.A.J. Englert, editors). Cambridge University Press, Cambridge, UK.
Shimizu, H., Watanabe, T., Henmi, T., Masuda, A., and Saito, H. (1988) Studies on allophane and imogolite by high resolution solid-state ^{29}Si- and ^{17}A1-NMR and ESR. *Geochemical Journal*, **22**, 23–31.
Shoji, S., Dahlgren, R., and Nanzyo, M. (1993) Genesis of volcanic ash soils. Pp. 37–71 in: *Volcanic Ash Soils. Genesis, Properties and Utilization* (S. Shoji, M. Nanzyo, and R. Dahlgren, editors). Elsevier, Amsterdam.
Tamura, K. and Kawamura, K. (2001) Molecular dynamics modeling of tubular aluminum silicate: imogolite. *The Journal of Physical Chemistry B*, **106**, 271–278.
Theng, B.K.G., Russell, M., Churchman, G.J., and Parfitt, R.L. (1982) Surface properties of allophane, halloysite, and imogolite. *Clays and Clay Minerals*, **30**, 143–149.
van der Gaast, S.J., Wada, K., Wada, S.-I., and Kakuto, Y. (1985) Small-angle X-ray powder diffraction, morphology, and structure of allophane and imogolite. *Clays and Clay Minerals*, **33**, 237–243.
Wada, K. (1967) A structural scheme of soil allophane. *American Mineralogist*, **52**, 690–708.
Wada, K. (1987) Minerals formed and mineral formation from volcanic ash by weathering. *Chemical Geology*, **60**, 17–28.
Wada, K. (1989) Allophane and imogolite. Pp. 1051–1087 in: *Minerals in Soil Environments* (J.B. Dixon and S.B. Weed, editors). Soil Science Society of America, Madison, Wisconsin, USA.
Wada, S.-I. and Wada, K. (1977) Density and structure of allophane. *Clay Minerals*, **12**, 289–298.
Wada, K., Henmi, T., Yoshinaga, N., and Patterson, S. H. (1972) Imogolite and allophane formed in saprolite of basalt on Maui, Hawaii. *Clays and Clay Minerals*, **20**, 375–380.
Wada, S.I., Eto, A., and Wada, K. (1979) Synthetic allophane and imogolite. *Journal of Soil Science*, **30**, 347–355.
Yoshinaga, N. and Aomine, S. (1962) Imogolite in some Ando soils. *Soil Science Plant Nutrition*, **8**, 22–29.

(*Received 28 March 2012; revised 11 February 2013; Ms. 664; AE: S. Petit*)